

Entanglement Density-Dependent Energy Absorption of Polycarbonate Films via Supersonic Fracture

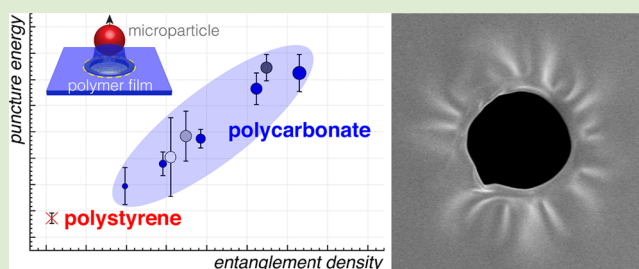
Edwin P. Chan,^{*,†,‡,§} Wanting Xie,^{‡,§,||} Sara V. Orski,[†] Jae-Hwang Lee,^{||} and Christopher L. Soles[†]

[†]Materials Science and Engineering Division, National Institute of Standards and Technology, Gaithersburg, Maryland 20899, United States

[§]Department of Physics and ^{||}Department of Mechanical and Industrial Engineering, University of Massachusetts, Amherst, Massachusetts 01003, United States

Supporting Information

ABSTRACT: The fracture behavior of glassy polymers is strongly coupled to molecular parameters such as entanglement density as well as extrinsic parameters such as strain rate and test temperature. Here we use laser-induced projectile impact testing (LIPIT) to study the extreme strain rate ($\approx 10^7$ s⁻¹) puncture behavior of free-standing polycarbonate (PC) thin films. We demonstrate that changes to the PC molecular mass and the degree of plasticization can lead to substantial changes in the specific puncture energy. We relate these changes to the alteration of the entanglement density of the polymer that determines the underlying failure mechanism as well as the size of the deformation zone.



For polymer glasses, it is well established that the number of entanglement junctions per chain, that is, entanglement density (ν_e), controls their failure mechanism.^{1–5} Entanglements restrict chain mobility relative to neighboring chains and thus dictate the extent of strain localization of the polymer.⁵ In brittle polymers such as polystyrene (PS) with a characteristically low entanglement density ($\nu_e \approx 4 \times 10^{24}$ entanglements/m³), crazing is observed in tension because the local ductility of PS chains is significantly high such that strain localization, in the form of void formation, is strongly favored. In other words, crazing is favored in PS because the crazing stress is lower than the yield stress ($\sigma_c \ll \sigma_y$).

Compared to PS, polycarbonate (PC) is a tough and transparent engineering thermoplastic with a much higher entanglement density ($\nu_e \approx 10^{26}$ entanglements/m³) that fails via a combination of shear deformation and crazing in tension. Shear deformation zones are typically observed directly ahead of the crack tip because crazing is disfavored ($\sigma_c \gg \sigma_y$) due to the significant molecular relaxations that suppress void formation. Above the yield point, the polymer strain hardens until $\sigma_c \approx \sigma_y$ at which point crazing occurs.

The effects of entanglement density on the fracture toughness of polymer glasses are established for quasi-static or low strain rate tests. However, increasing the strain rate significantly alters the mechanical behavior of polymers. A recent work⁶ on the ultra high rate ($\approx 10^7$ s⁻¹) puncture of ultrathin PS films indicated that a decrease in the film thickness enhances the specific puncture energy of the polymer. They suggested that, in this near surface region, the reduction in entanglement density enhances the ductility of the PS chains. This facilitates plastic deformation in the form of crazes and

unfibrillated deformation zones that significantly enhances energy absorption. As film thickness decreases, the near surface PS chains become an increasing fraction of the total film thickness, which leads to an increase in the specific puncture energy measured from LIPIT.

The question we would like to address is whether chain entanglements contribute to the failure mechanism of tough polymer glasses at extremely high strain rates. In this work, we use laser-induced projectile impact testing (LIPIT) to study the role of entanglement density on the high strain rate mechanical behavior of free-standing Bisphenol A-based PC thin films. We control the entanglement density of PC in two ways.⁷ The first is via changes to the molecular mass of the PC and the second is via the addition of Aroclor, a chlorinated biphenyl plasticizer for PC. Details of the sample preparation procedure are provided in the Supporting Information. Table 1 summarizes the thickness (h), the number (\bar{M}_n), and weight (\bar{M}_w) average molecular mass of the PC films studied using LIPIT. The plasticized PC series were prepared by combining the 15.9K PC with Aroclor 1260 at 5 mass %, 10 mass %, and 15 mass % Aroclor. As a reference, we prepared PS films for LIPIT testing using a similar sample preparation procedure. All the films were targeted to be ≈ 200 nm thick. We also conducted LIPIT measurements on the same materials at other thicknesses and did not see noticeable changes in the results.

Figure 1a is a schematic of the LIPIT instrument, which utilizes laser ablation of gold to propel a microparticle to

Received: April 9, 2019

Accepted: May 24, 2019

Table 1. Summary of Polycarbonate (PC) Film Properties Studied in This Work^a

sample	\bar{M}_n (kg/mol)	\bar{M}_w (kg/mol)	T_g (°C)	ρ_p (g/cm ³)	h (nm)	v_i (m/s)	A_{def} (μm ²)	v_c (m/s)	t_p (10 ⁻⁹ s)	$\Delta\epsilon/\Delta t$ (10 ⁷ s ⁻¹)
Molecular Mass Series										
8.3K	8.3 ± 0.3	25.2 ± 1.0	149	1.19	200 ± 8	508 ± 22	114 ± 13	≈743	≈8.1	≈2.9
11.4K	11.4 ± 0.2	38.0 ± 0.4	↓	↓	140 ± 9	483 ± 16	167 ± 12	≈719	≈10.1	≈2.2
14.8K	14.8 ± 0.5	48.2 ± 3.1			165 ± 6	514 ± 29	185 ± 19	≈749	≈10.2	≈2.3
15.9K	15.9 ± 2.1	59.3 ± 3.7			271 ± 2	513 ± 24	215 ± 14	≈748	≈11.1	≈2.1
26.0K	26.0 ± 0.4	59.3 ± 0.5			200 ± 6	504 ± 19	246 ± 36	≈740	≈12.0	≈1.9
Plasticized Series										
5% aro.	15.9 ± 2.1	59.3 ± 3.7	132	1.22	166 ± 8	513 ± 21	159 ± 26	≈748	≈9.5	≈2.5
10% aro.	15.9 ± 2.1	59.3 ± 3.7	116	1.24	143 ± 14	510 ± 23	108 ± 15	≈741	≈7.9	≈3.0
15% aro.	15.9 ± 2.1	59.3 ± 3.7	103	1.26	163 ± 11	503 ± 29	126 ± 18	≈732	≈8.6	≈2.7

^aThe glass transition temperatures (T_g) were obtained from Psurek et al.⁸ The error represents standard deviation of at least three measurements.

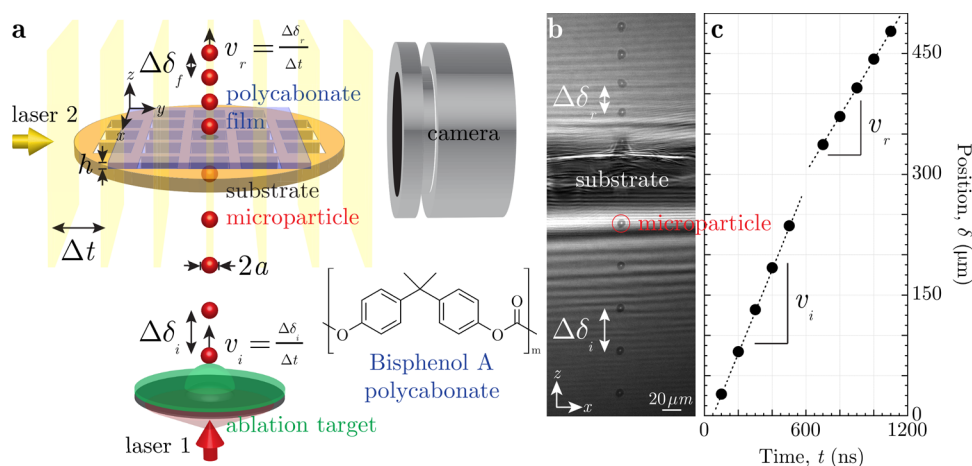


Figure 1. LIPIT experiment. (a) Schematic of the LIPIT instrument. The instrument utilizes laser-induced forward transfer to launch a 7.6 μm SiO₂ microparticle at supersonic velocity from the surface of a rapidly expanding polydimethylsiloxane (PDMS) membrane to puncture a free-standing thin polycarbonate (PC) film that is adhered to a TEM grid. (b) Stroboscopic image of the puncture event used to quantify the velocity profile of the microparticle. (c) Velocity profile of the microparticle illustrating the difference in the impact velocity (v_i) prior to puncture of the PC film and the residual velocity (v_r) following puncture.

supersonic velocity to puncture a free-standing polymer film. The ablation laser (laser 1) accelerates a single silica microparticle (diameter ($2a$) = 7.6 μm) that is placed on a polydimethylsiloxane (PDMS)/gold-coated glass plate near the focal point. The microparticle is accelerated by the rapid and large expansion of the PDMS membrane upon laser ablation. The microparticle diameter and velocity are measured via ultrafast (1 ps exposure time) stroboscopic imaging using pulsed white light (laser 2) and a complementary metal-oxide semiconductor (CMOS) camera (Figure 1). This imaging platform captures a single optical image that is composed of multiple exposures or “frames” of the particle puncturing the film (Figure 1b).

We use this image to compute the kinetic energy transfer (ΔE_k) of the puncture event, which is related to the impact and residual velocities of the microparticle (v_i , v_r)⁹

$$\Delta E_k = \frac{1}{2}m(v_i^2 - v_r^2) = E_p + E_{\text{drag}} \quad (1)$$

where E_p is the puncture energy and E_{drag} is energy loss due to air drag. The position of the particle (δ) is measured from the optical image. Since the time interval that was used ($\Delta t = 100$ ns) between each “frame” is determined by the repetition rate of the laser pulse, the velocity = $\Delta\delta/\Delta t$.

The LIPIT experiments were conducted in vacuum to minimize the effects of air drag. In the absence of air drag, ΔE_k

= E_p , with E_p encompassing the various dissipation mechanisms including elastic stretching, fracture, and adiabatic heating of the film. Since E_p also includes the kinetic energy transfer to the film and the removal of a plug of material, it is expressed as

$$E_p = \frac{\rho_p Ah}{2}v_i^2 + E_d \quad (2)$$

The first term is the minimum inelastic energy transfer to the material for a given h and puncture area, which is estimated by $A = \pi a^2$. The second term (E_d) represents all other energy dissipation mechanisms. To compare materials with different mass densities (ρ_p), the specific puncture energy is used instead as it is insensitive to the mass of the material ($\rho_p Ah$) in contributing to energy dissipation.

$$E_p^* = \frac{E_p}{\rho_p Ah} = \frac{v_i^2}{2} + E_d^* \quad (3)$$

Therefore, $E_d^* = E_d/\rho_p Ah$ is a metric for quantifying the extent of energy dissipation of a given material as the first term represents the lower limit of energy dissipation.

The strain rate ($\Delta\epsilon/\Delta t$) is a function of the radial rate of expansion of the deformed region of the polymer film,^{6,9} which is approximated as a cone-shaped expanding membrane of radius R_c ¹⁰

$$\frac{\Delta \varepsilon}{\Delta t} \cong \frac{\varepsilon_{\max}}{t_p} \cong \frac{t_p}{2} \left(\frac{v_i}{R_c} \right)^2 \quad (4)$$

where $\varepsilon_{\max} \cong (v_i t_p / R_c)^2 / 2$ is a 1-D approximation of the maximum tensile strain for an isotropic membrane experiencing biaxial deformation. The parameter, $t_p \cong R_c / v_c$ is the puncture time of the microparticle and is related to the cone velocity ($v_c \cong 1.23 c_{\parallel} (v_i / \sqrt{2} c_{\parallel})^{2/3}$), where $c_{\parallel} = \sqrt{E^* / \rho_p}$ is the in-plane speed of sound in the material that is a function of the plane-strain elastic modulus ($E^* = E / (1 - \nu^2)$) and mass density of the polymer.¹⁰

The strain is maximum near the center of impact, it decreases radially and reduces to zero at $\approx v_c t_p$. This 1-D model underestimates ε_{\max} because it assumes the mass of the local volume element responding to the propagating mechanical wave is held constant whereas the mass increases radially from the center of impact in a 2-D membrane. Thus, the actual radial strain profile is strongly localized around the puncture center and decreases faster than the prediction by this 1-D model.⁹ We use scanning electron microscopy (SEM) to quantify the postpuncture plastically deformed area (A_{def}) of each polymer film and estimate $R_c \approx \sqrt{A_{\text{def}} / \pi}$. Assuming the elastic modulus for bulk PC ($E^* \cong 3.5 \times 10^9 \text{ N/m}^2$), $c_{\parallel} \cong 1700 \text{ m/s}$ and $v_c \cong 734 \text{ m/s}$ for $v_i = 500 \text{ m/s}$. Thus, $\Delta \varepsilon / \Delta t$ ranges from $\approx 2 \times 10^7 \text{ s}^{-1}$ to $\approx 3 \times 10^7 \text{ s}^{-1}$.

The work of fracture of a material, closely approximated by the area beneath a stress vs strain curve, is enhanced with increasing volume of plastic deformation. This trend is observed in Figure 2 when we compare E_p^* with A_{def} . Top-down SEM micrographs of the punctured PC samples show that the molecular mass PC series all undergo shear yielding.

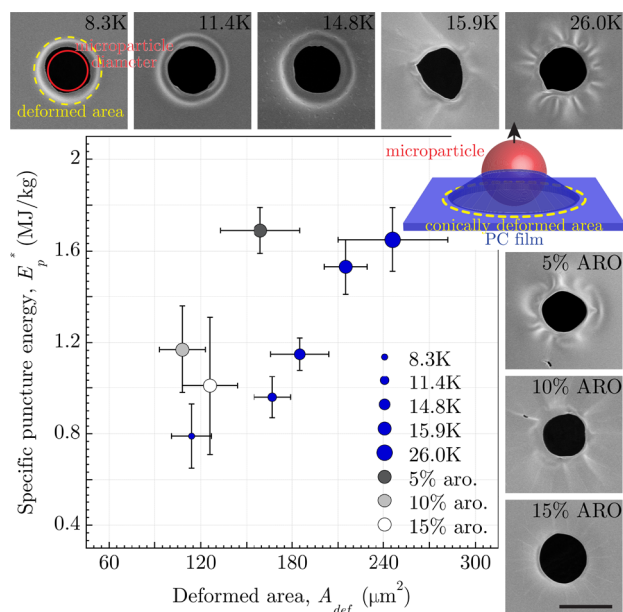


Figure 2. Specific puncture energy (E_p^*) vs plastically deformed area (A_{def}) for the molecular mass and the Aroclor plasticized PC series. The cartoon illustrates the deformation of the film during the puncture event and highlights the conically deformed area of the film. The top down SEM micrographs illustrate the deformation mechanism for all the PC samples post puncture. The error bars represent standard deviation of at least three measurements. Scale bar = 10 μm .

All of the samples have penetrated edges that appear to be near-circular with A_{def} that is larger than the cross-sectional area ($\approx 45 \mu\text{m}^2$) of the microparticle. There is a transition in the deformation mechanism for $\bar{M}_n > 14.8 \text{ kg/mol}$. The edges of the puncture appear quite smooth below this molecular mass (8.3K, 11.4K, and 14.9K) and the deformed area appears to be stretched along the radial direction. However, many deformation zones (DZs) appear for the two higher molecular mass PCs (15.9K and 26.0K) and the deformed area consists of folds reminiscent of surface wrinkles¹¹ that develop in thin films as a result of the balance in the bending vs stretching energies of the film due to an external but localized puncture force. We note that the wrinkles seen in this study are created by the impact-induced residual plastic deformation of the film without other external forces.

The plasticized PC series show a variety of failure behavior as a function of Aroclor content. The specific puncture energy for the 5 mass % Aroclor is slightly greater ($E_p^* = 1.69 \pm 0.10 \text{ MJ/kg}$) than the neat 15.9K PC ($E_p^* = 1.53 \pm 0.12 \text{ MJ/kg}$). Although both samples show similar failure deformation mechanisms with DZs around the penetrated edges, A_{def} for the 5 mass % is slightly lower than the neat PC, suggesting that either A_{def} is not a complete metric for assessing the extent of plastic deformation or other mechanisms contribute to E_p^* . Both radial crazes and DZs are observed for the 10 mass % Aroclor, whereas only radial crazes are observed for the 15 mass % Aroclor thus suggesting that there is a ductile-to-brittle transition around 10 mass % Aroclor. We note that since crazing is a high localized failure mechanism, the use of A_{def} for quantifying the size of the deformation region is rather difficult.

The linear increase in A_{def} with \bar{M}_n for the molecular mass PC series strongly suggests that plastic deformation is enhanced with increasing molecular mass of the polymer and this trend is shown in Figure 3a. The specific puncture energy ranges from $E_p^* = 0.79 \pm 0.14 \text{ MJ/kg}$ for 8.3K PC to $E_p^* = 1.65 \pm 0.14 \text{ MJ/kg}$ for 26.0K PC, which is significantly larger than PS ($E_p^* = 0.54 \pm 0.04 \text{ MJ/kg}$) of similar thickness but having significantly higher molecular mass ($\bar{M}_n = 101 \text{ kg/mol}$).

This trend can be explained with the aid of a high strain rate stress-strain curve for bulk PC (Figure 3b). The area under the stress-strain curve is a measure of the work of fracture of a material. An increase in the work of fracture for materials with similar yield strengths is attributed to the material's ability to sustain a larger strain until catastrophic failure occurs. For PC that possess a low entanglement molecular mass (M_c), significant plastic deformation occurs following yield when it first undergoes necking as the polymer chains are being drawn and aligned ahead of the crack tip. This is followed by strain stiffening due to physical chain entanglements that prevent further chain alignment. The development of a strain hardening modulus, which scales with the entanglement density ($G_h \sim \nu_c$),¹³ is characteristic of strain stiffening. We interpret E_p^* from LIPIT as a measure of the work of fracture of the material. This implies that the extent of the drawing/strain stiffening process of the PC film, that is, strain at failure, largely determines the extent of energy dissipation during puncture in LIPIT. The increase of \bar{M}_n is known to increase the propensity of PC to strain harden, and this effect is reflected by the increase in E_p^* .

Turning our attention to the Aroclor PC series, it is well-known that diluents such as Aroclor embrittle PC and significantly reduce the strain to failure. This has an opposite effect as increasing the propensity for strain hardening and

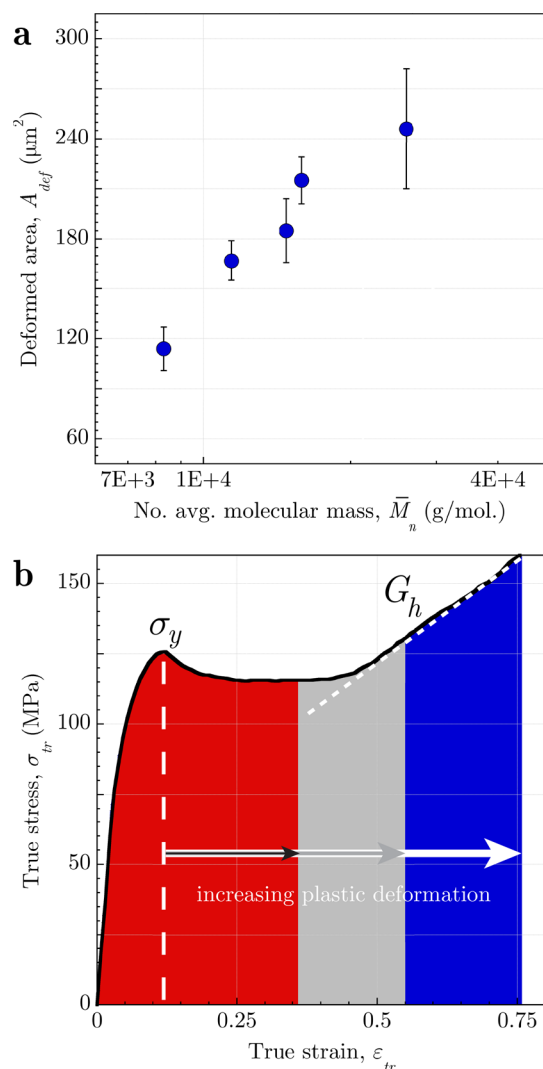


Figure 3. Deformed area (A_{def}) as a function of (a) number-average molecular mass (\bar{M}_n) of PC. The error bars represent standard deviation of at least three measurements. (b) Representative high strain rate mechanical behavior of bulk PC specimens in compression. Data taken from Sarva and Boyce.¹²

induces a ductile-to-brittle transition. The shape of the stress–strain curve for the plasticized PC is more consistent with a classic brittle fracture with little plastic deformation. As demonstrated in Figure 2, it is challenging to correlate A_{def} which is a projected area averaged around the punctured region, with E_p^* due to the difficulty in identifying the true interfacial regions of the film that has plastically deformed. Based on the simulations results of Hoy and Robbins that showed that strain hardening is a result of an increased plasticity with ϵ and ν_e at high rates,¹⁴ we instead use ν_e as a metric for quantifying plastic deformation. Specifically, we use Bersted’s entanglement model¹⁵ to estimate ν_e for our materials

$$\nu_e = \left(\frac{2\rho_p N_A}{3M_c} \left(1 - \frac{M_c}{\bar{M}_n} \right) \right) \quad (5)$$

where $M_c \approx 2M_e$, with $M_e \cong 1.8$ kg/mol corresponding to the entanglement molecular mass for PC with $M_e/\bar{M}_n \cong 8.8$.¹⁶

Since ρ_p and M_e for the plasticized PC series are not known, we approximate them by assuming that the increase in Aroclor content leads to proportional changes to these quantities, $\rho_p(x) \cong x_p \rho_p(0) + (1 - x_p) \rho_{aro}$ and $M_e(\phi_p) \cong M_{e,PC}/\phi_p$, where x_p is the mass fraction of PC, $\rho_p(0)$ is the density of the neat PC, as listed in Table 1, $\rho_{aro} = 1.57$ g/cm³ is the density of Aroclor,¹⁷ and $\phi_p \cong (x_p/\rho_p)/(x_p/\rho_p + (1 - x_p)/\rho_{aro})$ is the volume fraction of PC. Figure 4 shows that E_p^* is strongly correlated with ν_e for the materials investigated, suggesting that $E_p^* \propto \nu_e$.

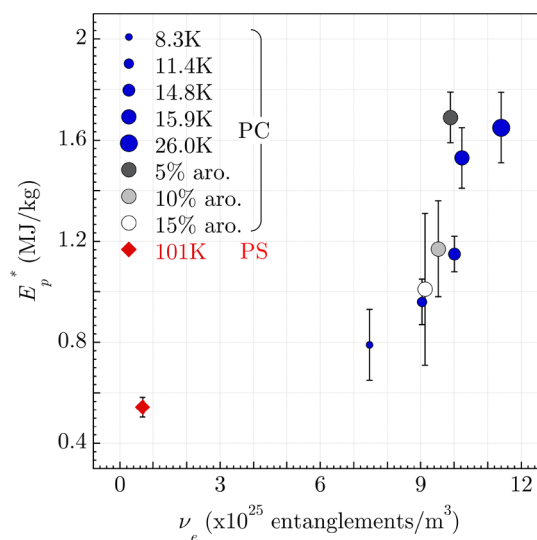


Figure 4. Specific puncture energy (E_p^*) vs entanglement density (ν_e) for both the molecular mass and the plasticized PC series. Also included is the result for PS. The error bars represent standard deviation of at least three measurements.

While \bar{M}_n for PS is significantly higher than that of the molecular mass PC series, the high M_e ($\cong 19.1$ kg/mol) results in an extremely low ν_e because $M_e/\bar{M}_n \approx 5.3$. It is not surprising that PS has the lowest E_p^* given that polymers with low entanglement density ($\nu_e < 4 \times 10^{25}$ entanglements/m³) fail via crazing.^{5,18} Polymers with $\nu_e > 8 \times 10^{25}$ entanglements/m³ are not able to form voids and fibrillate, they fail via shear deformation,⁵ which is exhibited by the molecular mass PC series. According to eq 5, all of the polymers studied here have \bar{M}_n that is well below the critical value ($\approx 50M_e$), where ν_e reaches a plateau value. The increase in \bar{M}_n will continue to raise ν_e and the associated enhancement in E_p^* due to increased plastic deformation.

The 5 mass % Aroclor samples fail via the formation of DZs. This result is consistent with the entanglement density scaling since modest additions of Aroclor lead to a proportional reduction in ν_e but not to the limit where crazing is observed. However, the 10 mass % and 15 mass % Aroclor samples appear to be inconsistent with this scaling as the SEM micrographs show the formation of crazes as opposed to the expected DZs. Steger et al. suggested that the incorporation of Aroclor can be viewed as inclusion of flaws/defects into the homogeneous PC material that enhances strain localization.¹⁹ Based on their argument, modest amounts of Aroclor (5 mass %) probably does not lead to the formation of a significant number of these high localized voids and crazing is not observed. However, larger amounts of plasticizer increases the

density of these flaws/voids, thereby increasing the propensity for craze formation since $\sigma_c \ll \sigma_y$.

In summary, our results demonstrate the role of entanglement density in polymer glasses on the energy dissipation in extremely high rate puncture events based on LIPIT. This mechanism of energy dissipation is unique to polymers due to their viscoelastic nature. This control is shown by the proportional change in the specific penetration energy with entanglement density via (1) increasing the molecular mass of the polymer or (2) reducing the plasticizer content that changes the size of the deformation region as well as dictate the specific failure mechanism. One important point we would like to make is that adiabatic heating can be substantial in LIPIT due to extensive shear deformation that leads to thermal softening and increased plasticity. It was suggested that the temperature rise for PS can reach as high as 400 °C.^{6,20} However, simulation results for PC show that it is unique compared to other polymer glasses in that adiabatic heating does not appear to contribute significantly to the high rate mechanical behavior.²¹ This may also help to explain the significantly higher E_p^* values seen in PC compared with PS since ν_e would be greatly reduced with adiabatic heating. Additionally, secondary relaxations such as β relaxations contribute significantly to the fracture toughness of PC at high testing rates as this molecular relaxation becomes accessible at around room temperature when $\Delta\epsilon/\Delta t > 10^2 \text{ s}^{-1}$.¹² One final point to note is that the relationship between ν_e and failure modes discussed here were established from quasi-static testing conditions. We expect that this relationship to change with deformation rate and we are currently establishing this relationship for PC using LIPIT. Besides ν_e , other molecular parameters, such as local chain stiffness that describes cooperative rearrangement, would need to be included to better describe the enhancement in E_p^* for PC and other polymer glasses in general. This is beyond the scope of the present manuscript, but we are currently developing measurement approaches that can quantify these relaxations.

■ ASSOCIATED CONTENT

Supporting Information

The Supporting Information is available free of charge on the ACS Publications website at DOI: 10.1021/acsmacrolett.9b00264.

Materials, experimental details, and derivations (PDF)

■ AUTHOR INFORMATION

Corresponding Author

*E-mail: edwin.chan@nist.gov.

ORCID

Edwin P. Chan: 0000-0003-4832-6299

Wanting Xie: 0000-0002-0151-6362

Jae-Hwang Lee: 0000-0002-2546-1044

Author Contributions

[‡]These authors contributed equally to this work.

Notes

The authors declare no competing financial interest.

■ ACKNOWLEDGMENTS

The authors thank Dr. Shawn Chen and Dr. Amanda Souna for providing feedback on the manuscript. J.H.L. and W.X. gratefully acknowledge financial support from the U.S. Army

Research Laboratories under the Grant No. W911NF-15-2-0026. This work is a contribution of NIST, an agency of the U.S. Government, and not subject to U.S. copyright.

■ REFERENCES

- (1) Aharoni, S. M. Correlations between chain parameters and failure characteristics of polymers below their glass transition temperature. *Macromolecules* **1985**, *18*, 2624–2630.
- (2) Donald, A. M.; Kramer, E. J. Effect of molecular entanglements on craze microstructure in glassy polymers. *J. Polym. Sci., Polym. Phys. Ed.* **1982**, *20*, 899–909.
- (3) Donald, A. M.; Kramer, E. J. The competition between shear deformation and crazing in glassy polymers. *J. Mater. Sci.* **1982**, *17*, 1871–1879.
- (4) Haward, R. N., Ed. In *Physics of Glassy Polymers*, 2nd ed.; Springer: Netherlands, 1997.
- (5) Whitten, P. G.; Brown, H. R. Polymer entanglement density and its influence on interfacial friction. *Phys Rev E Stat Nonlin Soft Matter Phys.* **2007**, *76*, 026101.
- (6) Hyon, J.; Lawal, O.; Fried, O.; Thevamaran, R.; Yazdi, S.; Zhou, M.; Veysset, D.; Kooi, S. E.; Jiao, Y.; Hsiao, M.-S.; Streit, J.; Vaia, R. A.; Thomas, E. L. Extreme Energy Absorption in Glassy Polymer Thin Films by Supersonic Microprojectile Impact. *Mater. Today* **2018**, *21*, 817–824.
- (7) Certain instruments and materials are identified in this paper to adequately specify the experimental details. Such identification does not imply a recommendation by the National Institute of Standards and Technology, nor does it imply that the materials are necessarily the best available for the purpose.
- (8) Psurek, T.; Soles, C. L.; Page, K. A.; Cicerone, M. T.; Douglas, J. F. Quantifying Changes in the High-Frequency Dynamics of Mixtures by Dielectric Spectroscopy. *J. Phys. Chem. B* **2008**, *112*, 15980–15990.
- (9) Lee, J.-H.; Loya, P. E.; Lou, J.; Thomas, E. L. Dynamic mechanical behavior of multilayer graphene via supersonic projectile penetration. *Science* **2014**, *346*, 1092–1096.
- (10) Phoenix, S. L.; Porwal, P. K. A new membrane model for the ballistic impact response and V50 performance of multi-ply fibrous systems. *Int. J. Solids Struct.* **2003**, *40*, 6723–6765.
- (11) Huang, J.; Juskiewicz, M.; de Jeu, W. H.; Cerda, E.; Emrick, T.; Menon, N.; Russell, T. P. Capillary Wrinkling of Floating Thin Polymer Films. *Science* **2007**, *317*, 650–653.
- (12) Sarva, S.; Boyce, M. Mechanics of polycarbonate during high-rate tension. *J. Mech. Mater. Struct.* **2007**, *2*, 1853–1880.
- (13) Rottler, J. Fracture in glassy polymers: a molecular modeling perspective. *J. Phys.: Condens. Matter* **2009**, *21*, 463101.
- (14) Hoy, R. S.; Robbins, M. O. Strain hardening of polymer glasses: Effect of entanglement density, temperature, and rate. *J. Polym. Sci., Part B: Polym. Phys.* **2006**, *44*, 3487–3500.
- (15) Bersted, B. H. Entanglement network model relating tensile impact strength and the ductile-brittle transition to molecular structure in amorphous polymers. *J. Appl. Polym. Sci.* **1979**, *24*, 37–50.
- (16) Plummer, C. J. G.; Soles, C. L.; Xiao, C.; Wu, J.; Kausch, H.-H.; Yee, A. F. Effect of Limiting Chain Mobility on the Yielding and Crazing Behavior of Bisphenol-A Polycarbonate Derivatives. *Macromolecules* **1995**, *28*, 7157–7164.
- (17) https://pubchem.ncbi.nlm.nih.gov/compound/2_2_3_3_4_4_-hexachlorobiphenyl#section=Top.
- (18) Henke, C. S.; Kramer, E. J. Crazing and shear deformation in crosslinked polystyrene. *J. Polym. Sci., Part B: Polym. Phys.* **1996**, *34*, 2825–2841.
- (19) Steger, T. R.; Schaefer, J.; Stejskal, E. O.; McKay, R. A. Molecular Motion in Polycarbonate and Modified Polycarbonates. *Macromolecules* **1980**, *13*, 1127–1132.
- (20) Estevez, R.; Basu, S.; Van der Giessen, E. In *European Structural Integrity Society*; Blackman, B. R. K., Pavan, A., Williams, J. G., Eds.; Elsevier, 2003; Vol. 32; pp 155–165.

(21) Kendall, M. J.; Siviour, C. R. Experimentally simulating high-rate behaviour: rate and temperature effects in polycarbonate and PMMA. *Philos. Trans. R. Soc., A* **2014**, *372*, 20130202.